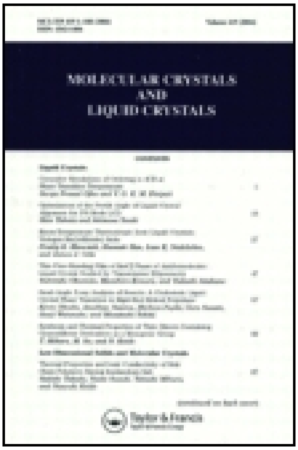

Molecular Crystals and Liquid Crystals
Publication details, including instructions for authors and subscription information:
http://www.tandfonline.com/loi/gmcl20

Electrooptical Switching in Homeotropically Aligned Cell Geometry of Ferroelectric Liquid Crystal

Jae Shin Jo [a] , Masanori Ozaki [a] & Katsumi Yoshino [a]
[a] Department of Electronic Engineering, Graduate School of Engineering, Osaka University, Suita, Osaka, Japan

Version of record first published: 18 Oct 2010

Mol. Cryst. Liq. Cryst., Vol. 410, pp. 191/[719]–200/[728], 2004

ISSN: 1542-1406 print/1563-5287 online
DOI: 10.1080/15421400490436331

ELECTROOPTICAL SWITCHING IN HOMEOTROPICALLY ALIGNED CELL GEOMETRY OF FERROELECTRIC LIQUID CRYSTAL

Jae Shin Jo, Masanori Ozaki, and Katsumi Yoshino
Department of Electronic Engineering, Graduate School of Engineering, Osaka University, 2-1 Yamada-oka, Suita, Osaka 565-0871, Japan

Electrooptic characteristics based on the deformation of helical structure in a homeotropically aligned ferroelectric liquid crystal have been studied. In the voltage range below the threshold for the disappearance of the helix, no hysteresis was observed in the voltage dependence of the transmission intensity curve. Wide viewing angle characteristics can be obtained by improving an electrode configuration in a homeotropically aligned cell.

Keywords: FLC; homeotropic alignment; viewing angle

INTRODUCTION

Many types of electrooptic effects have previously been proposed in a ferroelectric liquid crystal (FLC) [1 ∼ 5]. They can be classified into two types of effects; one originates from light scattering such as the deformation of helical structure (DHS) [1] and transient scattering mode (TSM) [2], and the other is based on a birefringence change such as the surface stabilized ferroelectric liquid crystal (SSFLC) [3], the soft mode type (SMFLC) [4] and the deformed helical ferroelectric type (DHF) [5]. However most of them are based on planer cell geometry in which the smectic layers are in principle perpendicular to the substrate. So far few studies have been reported on electrooptic effects utilizing the so-called homeotropically aligned cell geometry, in which the smectic layers are parallel to the substrate [6,7]. In this cell geometry, the electric field is applied parallel to the substrates in a similar manner to that of an in-plane switching (IPS) of nematic liquid crystals.

Address correspondence to Jae Shin Jo, Department of Electronic Engineering; Graduate School of Engineering, Osaka University, 2-1 Yamada-oka, Suita, Osaka 565-0871, Japan.

Ozaki *et al.* have proposed two types of electrooptic effects in the homeotropically aligned cell of FLC [7]. In one of them, the deformation of helical structure upon the application of an in-plane electric field in the cell placed between crossed polarizers is used.

In this paper, we present in detailed the characteristics such as the transmission hysteresis, angular dependence and response speed in a homeotropically aligned FLC cell. We also report a new configuration of the electrode which improves viewing angle characteristics in this cell.

EXPERIMENTAL

The FLC material used in this study was (2S,3S)-3-methyl-2-chloropentanoic acid 4′,4″-octyloxybiphenyl ester (3M2CPOOB) [8,9], which has a large spontaneous polarization (300 nC/cm^2 at 35°C). The helical pitch is about 3 μm. The molecular structure of this material is shown below.

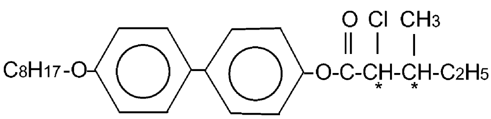

The preparation method and fundamental electrical and optical properties have previously been reported [9,10].

The compound was inserted into a sandwich cell consisting of two glass plates. In order to realize a homeotropic alignment of the liquid crystal molecules, the surfaces of the glass substrates were coated with a polyimide (JALS-2021-R2, JSR). Figure 1 shows the cell configuration used in this study. Aluminum foils were used as both the electrode and the spacer. The electric field can be applied field parallel to the cell surfaces and smectic layers. The electrode interval was 1.1 mm. The cell gap was 12 μm. The cell was placed between crossed polarizers. The direction of the applied electric field along the y-axis makes an angle of 45° to the polar-

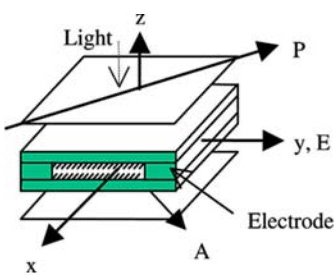

FIGURE 1 The device configuration used in this study. (See COLOR PLATE I)

ization direction of the polarizer. As a light source for the electrooptic measurement, a He–Ne laser light (632.8 nm) was used.

For the measurement of viewing angle characteristics, an inter-digital electrode was used. Polyester films were used as the spacer. The cell gap was 25 µm and the electrode distance was 100 µm.

RESULTS AND DISCUSSION

Figure 2 shows a schematic explanation of the electrooptic switching in the homeotropic aligned FLC cell. In the absence of an electric field ($E = 0$), a helical structure whose axis is perpendicular to the substrates is formed. Namely, the FLC molecules, which tilt with respect to the smectic layer normal (z-axis), rotate around the axis from one layer to the next. In this helical structure, the projection of the optical axis on the cell surface also rotates around the z-axis with a pitch much less than cell thickness, resulting in the disappearance of the macroscopic birefringence between the crossed polarizers except for a slight optical rotatory power. Consequently, the light transmission is almost zero under the no field condition.

When the electric field is applied above a threshold E_c, the helical structure disappears and the spontaneous polarization orients along the field (y-axis), and the FLC molecules align perpendicular to the field. As a result, the projection direction of the optical axis on the substrates points to the x-axis and makes an angle of 45° to the polarization direction of the

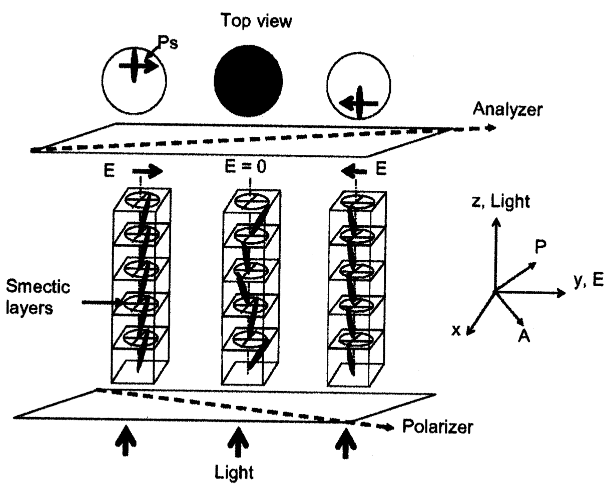

FIGURE 2 The schematic explanation of switching mechanism in homeotropically aligned FLC.

polarizer. Consequently, a high transmission state is realized above the threshold.

Figure 3(a) shows the applied voltage dependence of the transmission light intensity (*T.I.*) for 3M2CPOOB at 49°C. The triangular waveform of the voltage at 5 mHz was applied. At $V = 0$, that is an initial state, *T.I.* is almost zero. In the absence of the electric field, a helical structure whose axis is perpendicular to the substrates is formed. Consequently, the light transmission is almost zero under the no field.

When the voltage increases from 0 V, *T.I.* monotonically increases and levels off at voltages higher than 15 V. This should be attributed to the disappearance of the helical structure. Consequently, the high transmission state is realized above the threshold.

When the voltage is subsequently lowered, the high transmission state is maintained until zero voltage. Once the polarity of the applied voltage is reversed, *T.I.* decreases steeply. Namely, the hysteresis is observed in a *V-T.I.* curve. The profile of this hysteresis depends on the temperature, scan rate of the voltage and cell thickness.

Figure 3(b) shows the *T.I.* curve at 49°C, when the maximum applied voltage is limited below the unwinding threshold of the helical structure (<8 V). When a voltage of approximately above 8 V is applied, the hysteresis is observed in the *V-T.I.* curve as shown in Figure 3(a). However, when the applied voltage is below 8 V, the *V-T.I.* curve shows no hysteresis as shown in Figure 3(b).

Figure 4 shows the temperature dependence of the threshold voltage which does not cause hysteresis in the *V-T.I.* curve. With decreasing

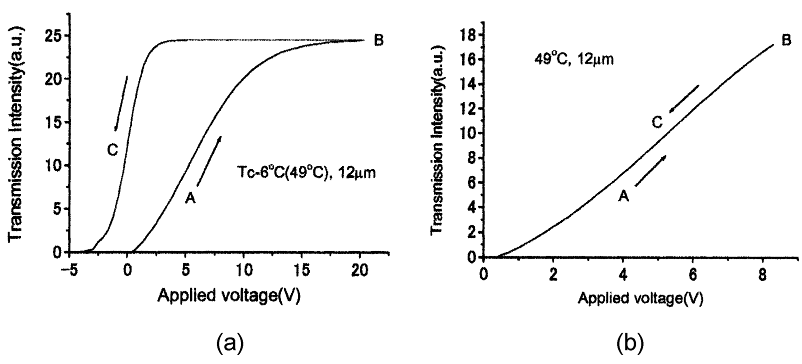

FIGURE 3 (a) Voltage dependence of the transmission intensity at 49°C. The voltage above the threshold for unwinding the helix is applied. (b) Voltage dependence of the transmission intensity in a non-hysteresis operation in which the voltage below the threshold for unwinding the helix is applied.

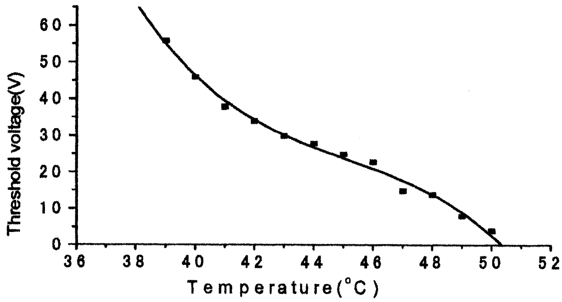

FIGURE 4 Temperature dependence of the threshold voltage for the non-hysteresis operation.

temperature, the threshold voltage increases. The critical field for the unwinding of the helical structure E_c is represented as the following equation [11],

$$E_c = \frac{\pi^4 K \sin^2 \theta}{4P_s \cdot p^2} \tag{1}$$

where K is the elastic constant, θ is the tilt angle, p is the pitch of the helical structure and P_s is the spontaneous polarization. K, θ and $1/p$ increase with decreasing temperature.

Although P_s increases with decreasing temperature, the contribution of P_s to the temperature dependence of E_c is compensated by that of θ because P_s is proportional to θ according to a simple phenomenological calculation. In addition, the p of the FLC material used in this study is almost constant in the whole temperature range of the chiral smectic-C phase except for the vicinity of the phase transition point. Therefore, if the temperature dependence of these parameters is taken into account, E_c should increase at lower temperature as shown in Figure 4.

The dynamic characteristics of the electrooptic effect in the homeotropically aligned cell have been studied. Figure 5(a) shows typical waveforms of the transmission intensity change upon applying a stepwise voltage. Figure 5(b) shows the voltage dependence of the response time at 48°C. The response time is defined as the time required for switching from 10% to 90% of the transmission change. It was found that the response time decreases with increasing voltage.

Neglecting the contribution of dielectric anisotropy, the torque balance equation for an azimuthal angle φ of P_s about the helix axis can be written as,

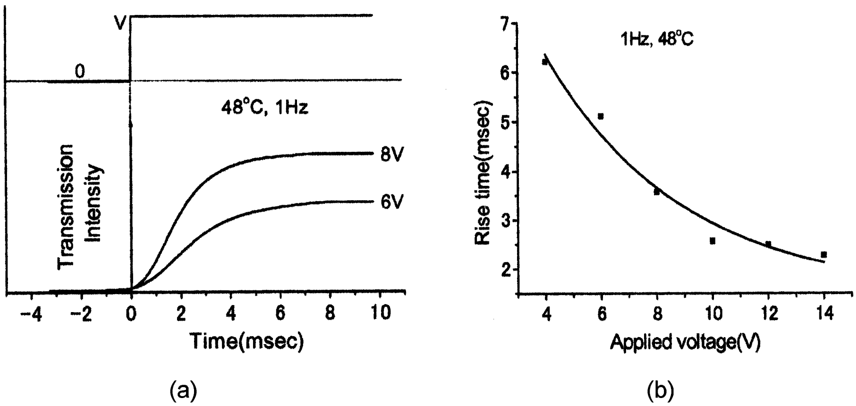

FIGURE 5 (a) Typical optical response waveforms to the stepwise voltage. (b) Voltage dependence of the rise time at 48°C.

$$K\nabla^2\varphi - P_sE\sin\varphi = \eta\frac{\partial\varphi}{\partial t} \tag{2}$$

where η is rotational viscosity. Resolving this balance equation, the response time τ is given as,

$$\tau \cong \frac{\eta}{Kq^2 + P_sE} \tag{3}$$

where q is the helix wave vector which is defined as $q = 2\pi/p$ using the helical pitch p. In our system studied here, the applied electric field is not so high; $E < 100\,\mathrm{V/cm}$. 3M2CPOOB has P_s of about $140\,\mathrm{nC/cm^2}$ at 48°C and the helical pitch of about 3 μm. If we assume K to be 3×10^{-12} N, Kq^2 and P_sE are estimated to be $13\,\mathrm{J/m^2}$ and $14\,\mathrm{J/m^2}$, respectively. Therefore, the elastic torque is not negligible in the dynamic response of the electrooptic effect and the field dependence of τ does not follow the simple relationship, $\tau \approx 1/E$ which is generally applied to a surface stabilized ferroelectric liquid crystal (SSFLC).

As is evident from Eq. (3), a faster response can be obtained by using a material with a short helical pitch. In addition, if we use the short pitch material, a higher field can be applied for the operation because the threshold field E_c for unwinding the helix is high, resulting in the faster response.

Figure 6 shows the voltage dependence of the decay time at 48°C. The decay time decreases with increasing applied voltage. However, above 10 V (E:90 V/cm, electrode gap:1.1 mm), the decay time is almost independent of the voltage. This result is associated with a hysteresis curve of the transmission light intensity. The threshold voltage that does not cause hysteresis

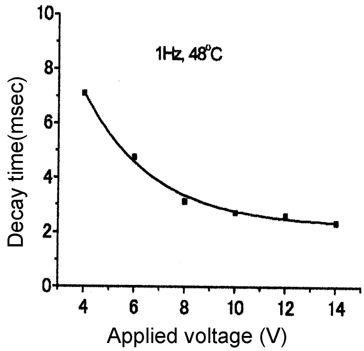

FIGURE 6 Applied voltage dependence of the decay time at 48.

is about 10 V at 48°C of 3M2CPOOB. Therefore, in the voltage range above 10 V in which the helical structure is unwound and hysteresis curve is observed. In such a unwound state, the decay time does not depend on the applied voltage. The response time required for the formation of the helical structure is represented by a simple equation, $\tau \cong \eta/Kq^2$. As is evident from this equation, the decay time is independent of the applied electric field.

Figure 7 shows the voltage dependence of the transmission light intensity as a function of the incidence angle of light. The sandwich cell of 3M2CPOOB is placed between the crossed polarizers, and is rotated around two axes; the directions along the electric field (y-axis) and perpendicular

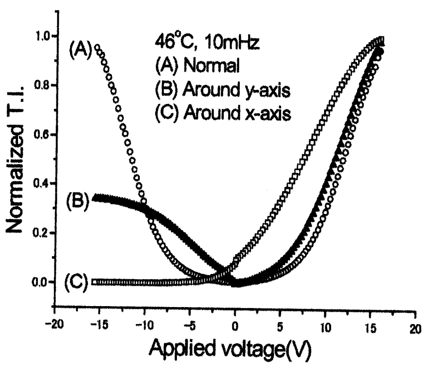

FIGURE 7 Voltage dependence of the transmission light intensity (*T.I.*) at various incidence directions of light. The cell is rotated around the y-axis (B) and the x-axis (C).

to the field (x-axis) as shown in Figure 1. The triangular wave of voltage at 10 mHz was applied at 46°C. The applied voltage is within the range of nonhysteresis operation as shown in Figure 3(b).

For the normal incidence (A), the *V-T.I.* curve is symmetry with respect to $V = 0$ as shown in Fig. 7. When the cell is rotated by 20° around the y-axis parallel to the applied field E, the *V-T.I.* curve is slightly deformed (B) and the voltage showing the *T.I.* maximum shifts to higher voltage. The curve (C) shows the transmission light intensity when the cell is rotated by 20° around the x-axis perpendicular to the applied electric field E. The *T.I.* curve shows a unipolar behavior. Although *T.I.* increases with increasing voltage ($V > 0$), at negative voltage, *T.I.* is almost zero independent of the applied voltage. Even at 0 V, non-zero transmission occurs. Therefore at negative voltage, a contrast inversion occurs. When the voltage is applied, the average optical axis tilts in the x-z plane perpendicular to the electric field toward the direction corresponding to the field polarity. Therefore, if the light propagates obliquely in the x-z plane, *T.I.* should strongly depend on the incident direction. This asymmetric angular dependence of *T.I.* is improved by considering the electrode configuration.

Figure 8(a) shows the viewing angle characteristic in the cell with a common inter-digital electrode structure. It is found that the contrast ratio strongly depend on the viewing angle.

In order to improve a viewing angle characteristic, we propose new electrode geometry as shown in Figure 9(a). The improved electrode geometry

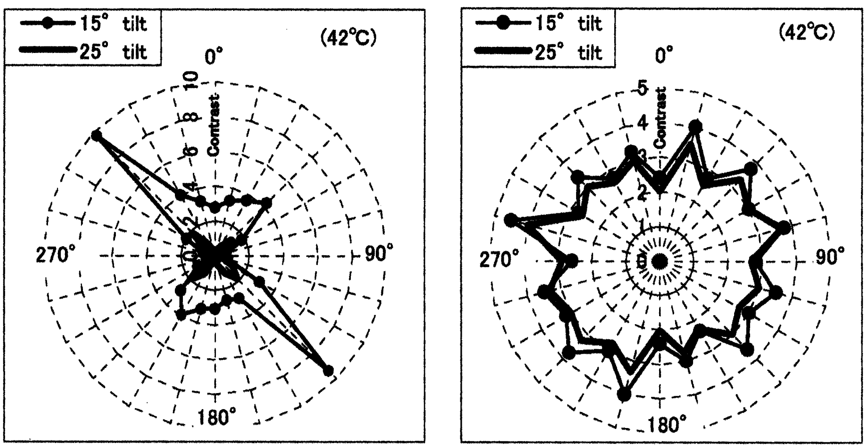

FIGURE 8 (a) The viewing angle characteristic in the common inter-digital electrode geometry. (b) The viewing angle characteristic in the improved V-shaped electrode geometry as shown in Figure 9(a).

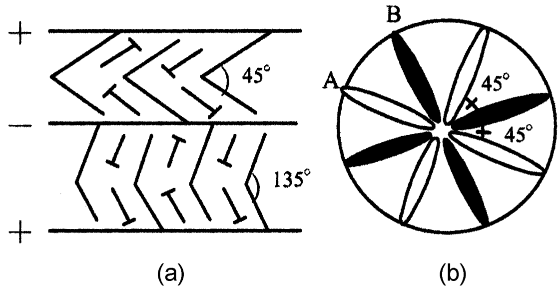

FIGURE 9 (a) The improved new electrode geometry. (b) The tilt directions of the liquid crystal molecules under the electric field, which point to all direction in the substrate plane.

contains two types of V-shaped inter-digital electrodes with apex angles of 45° and 135°. These V-shaped electrodes of 45° and 135° are arranged with alternation.

Figure 9(b) shows a schematic explanation of the molecular tilt directions between these electrodes. [A] and [B] correspond to the projections on a substrate of tilted molecules between 45°-V and 135°-V electrodes, respectively. This suggests that the molecules should tilt homogeneously to all directions when the electric field is applied.

Figure 8(b) shows the viewing angle characteristics for the cell with the improved electrode geometry as shown in Figure 9(a). It is found that the viewing angle characteristic is improved compared with that in the common inter-digital electrode cell. This should be attributed to the homogeneous distribution of molecular tilt in the improved electrodes as shown in Fig. 9(b).

CONCLUSIONS

The electrooptic characteristics in the homeotropically aligned FLC device were investigated. In the voltage range below the threshold for the disappearance of the helix, no hysteresis was observed in the *V-T.I.* curve. The viewing angle characteristic of *T.I.* could be improved by using the V-shaped electrode configurations.

REFERENCES

[1] Yoshino, K., Balakrishnan, K. G., Uemoto, T., Iwasaki, Y., & Inuishi, Y. (1978). *Jpn. J. App. Phys.*, *17*, 597.
[2] Yoshino, K. & Ozaki, M. (1984). *Jpn. J. Appl. Phys.*, *23*, L385.

[3] Clark, N. A. & Lagerwall, S. T. (1980). *Appl. Phys. Lett.*, *36*, 899.
[4] Anderson, G., Dahl, I., Keller, P., Kuczynski, W., Lagerwall, S. T., Skarp, K., & Stebler, B. (1987). *Appl. Phys. Lett.*, *51*, 640.
[5] Beresnev, L. A., Blinov, L. M., & Dergacheve, D. I. (1988). *Ferroelectrics*, *85*, 173.
[6] Kuczynski, W. & Hoffmann, J. (1984). *Ferroelectrics*, *59*, 117.
[7] Ozaki, M., Tagawa, A., Sadohara, Y., Oda, S., & Yoshino, K. (1991). *Jpn. J. Appl. Phys.*, *30*, 2366.
[8] Sakurai, T., Mikami, N., Higuchi, R., Ozaki, M., & Yoshino, K. (1986). *J. Chem. Soc. Chem. Commun.*, 978.
[9] Yoshino, K., Kishio, S., Ozaki, M., Sakurai, T., Mikami, N., & Higuchi, R. (1986). *Jpn. J. Appl. Phys.*, *25*, L416.
[10] Ozaki, M., Yoshino, K., Sakurai, T., Mikami, N., & Higuchi, R. (1987). *J. Chem. Phys.*, *86*, 3648.
[11] Martinot-Lagarde, Ph. (1981). *Mol. Cryst. Liq. Cryst.*, *66*, 61.